Available online at www.sciencedirect.com
SCIENCE DIRECT®

Journal of the European Ceramic Society 24 (2004) 2023–2029

www.elsevier.com/locate/jeurceramsoc

Electron energy-loss spectroscopy (EELS) studies of an yttria stabilized TZP ceramic

I.M. Ross[a,*], W.M. Rainforth[a], A.J. Scott[b], A.P. Brown[b], R. Brydson[b], D.W. McComb[c]

[a]*Department of Engineering Materials, University of Sheffield, Sheffield S1 3JD, UK*
[b]*Institute for Materials Research, University of Leeds, Leeds LS2 9JT, UK*
[c]*Department of Chemistry, University of Glasgow, Glasgow G12 8QQ, UK*

Received 15 January 2003; received in revised form 2 May 2003; accepted 10 May 2003

Abstract

Electron energy-loss spectroscopy (EELS) was used to examine the distribution of zirconia polymorphs within a sintered 3Y–TZP ceramic prepared by co-milling via detailed analysis of the energy-loss near-edge structure (ELNES) at the oxygen K-edge. Measurement of the peak positions and the overall shape of the fine structure in the oxygen K ELNES clearly facilitates the differentiation between the cubic, tetragonal and monoclinic zirconia phases within the bulk material. Examination of t–ZrO_2:t–ZrO_2 grain–boundary interfaces revealed significant co-segregation of the cation dopants Al^{3+} and Y^{3+}. However, the ELNES at the oxygen K-edge exhibited characteristics which suggest that the oxygen coordination at the boundary interface is similar to that of the bulk tetragonal grains for the volume sampled by the electron beam.

Keywords: Electron energy-loss spectroscopy (EELS); Energy-loss near-edge structure (ELNES); Grain–boundaries; ZrO_2

1. Introduction

The technological significance of zirconia-based ceramics for engineering applications is well established.[1] Tetragonal zirconia polycrystals (TZPs) have attracted particular attention due to their high toughness, as a consequence of the martensitic phase transformation of the metastable tetragonal phase to the monoclinic structure (transformation toughening).[2] Zirconia can exhibit three well-defined polymorphic forms at ambient pressure: the monoclinic (m-ZrO_2) phase (space group $P2_1/c$) which is stable up to ~1170 °C; the tetragonal (t-ZrO_2) phase ($P\bar{4}m2$) which is stable up to ~2370 °C, and the cubic (c-ZrO_2) phase ($Fm3m$) which is stable up to the melting temperature of 2680 °C. In the pure material only the monoclinic form is stable at room temperature. However, the tetragonal and cubic phases may be retained at low temperature by the addition of suitable stabilisers such as Y_2O_3, CaO, MgO and CeO_2. For yttria-stabilised TZPs, the microstructure of the sintered material is dependent on the homogeneity of the precursor and on the sintering conditions.[3] Inhomogeneous stabiliser distribution, or sintering in the $(c+t)$-ZrO_2 phase field can lead to a mixture of t-ZrO_2 and c-ZrO_2 within the final sintered compact, which are not readily differentiated by conventional selected area electron diffraction (SAED) or X-ray diffraction as a consequence of their very similar lattice parameters.[4] The cubic phase grains are often physically larger than those of the tetragonal phase and this is frequently used to distinguish the two. However, the cubic phase can also exist as finer grains, which are not easy to distinguish from the tetragonal phase by morphology alone and this can introduce substantial errors to this subjective method for measuring volume fractions of the phases present.[1] Recent studies by Selulic et al.[5] have demonstrated that it is possible to distinguish c-ZrO_2 from t-ZrO_2 using Raman Spectroscopy, but this is limited by the current spatial resolution of around 1–2 μm.

Interest in the application of electron energy-loss spectroscopy (EELS) to the study of zirconia has increased in recent years.[6–10] The electron energy-loss near edge structure (ELNES) of a specific edge within an energy-loss spectrum is known to be sensitive to the chemical environment of the atom undergoing excitation and hence, when performed within the environment

* Corresponding author. Tel.: +44-114-222-5811; fax: +44-114-222-5943.
E-mail address: i.ross@shef.ac.uk (I.M. Ross).

0955-2219/03/$ - see front matter © 2003 Elsevier Ltd. All rights reserved.
doi:10.1016/S0955-2219(03)00375-3

of a transmission electron microscope (TEM), the technique offers the potential to probe the local structure of a material at the nanometre scale.[11] Previous work by McComb[6] has shown that differences in the local environment surrounding the oxygen atoms of the three common ZrO_2 phases are reflected in the ELNES of the oxygen K-edge (for phase pure powders) thus providing a fingerprint with which to distinguish between the different phases. Subsequently, detailed theoretical calculations by Ostanin et al.[12] have demonstrated that the O K-ELNES is sensitive to the dopants and vacancies present in stabilised zirconias. These studies have focussed on comparing theoretical ELNES with experimental data derived from model powder systems. The aim of this current report is to illustrate the use of ELNES in the study of a dense multiphase sintered zirconia ceramic, where the constraint induced by the surrounding matrix plays an additional role in phase retention, in addition to the chemical effect apparent in both powders and dense ceramics.

2. Experimental

A sintered 3Y-TZP ceramic was prepared from a commercial 3Y-ZrO_2 powder (YZ5N Tioxide Specialties, UK) manufactured by the plasma decomposition of $ZrCl_4$ and subsequent co-milling with 3 mol% Y_2O_3 with a nominal composition of 5.2 wt.% Y_2O_3, 0.15 wt.% Al_2O_3, 1.9 wt.% HfO_2, <0.01 wt.% SiO_2, <0.01 wt.% Fe_2O_3 and <0.01 wt.% Na_2O_3. Compacts were produced by uniaxial pressing (20 MPa) and subsequently cold isostatic pressing at 400 MPa before being sintered at 1450 °C in air for 3 h.[9] Specimens for TEM analysis were prepared by the conventional method of mechanical thinning followed by argon ion beam milling to electron transparency. For comparison, standard *m*-ZrO_2 (TZ0 Tosoh Corporation), *t*-ZrO_2 (3 mol% Y_2O_3), and *c*-ZrO_2 (10 mol% Y_2O_3) zirconia powders (MEL Chemicals) were also prepared for TEM analysis, by dispersion in ethanol onto holey carbon supports. Energy-loss spectroscopy (EELS) was performed (in parallel) in a JEOL 2010F and Philips CM200F field emission TEMs, both operating at 200 kV and equipped with GATAN Imaging Filters (GIF200). Both instruments are capable of generating useful analytical probes of 1–2 nm diameter and provide a routine energy resolution for EELS studies of 0.8 eV.

Energy-loss spectra were acquired in image coupling mode.[13] Spectrometer energy dispersions of 0.1 eV/channel (oxygen K-edge) and 0.5 eV/channel (Y and Zr $L_{2,3}$-edges) were used with convergence and collection semi-angles of 8.5 and 4.8 mrad (JEOL 2010F) and 1.0 and 6.9 mrad (Philips CM200F) respectively. Grain boundary studies were performed exclusively on the JEOL 2010F using an electron probe of nominally 1 nm diameter. For each data set, a low loss spectrum including the zero loss peak (ZLP), was also recorded using the same spectrometer energy dispersion. All EELS data were subsequently corrected for the spectrometer dark current and pixel to pixel gain variations (using the automated routines within the image filter controls). After subtraction of a background of the form AE^{-r}, plural scattering contributions were deconvoluted from the core loss spectra using the Fourier ratio method. Finally, the point spread function of the detector was deconvoluted from the spectra.[13] A corresponding energy dispersive X-ray (EDX) spectrum was acquired for each energy-loss spectrum via an Oxford/Link ISIS X-ray spectrometer using a 50 second preset live time acquisition. Quantification of subsequent EDX data was performed using the Cliff-Lorimer Thin-Section technique, assuming an average material density of 6.0 g/cm^3 and a specimen thickness derived from the appropriate EELS low loss spectrum as described by Egerton.[13]

3. Results and discussion

3.1. Analysis of grain interiors

The previous work of McComb[6] has identified distinct differences in the oxygen K-ELNES of the different zirconia polymorphs, enabling the cubic, tetragonal and monoclinic zirconia phases to be distinguished for phase pure powders. Fig. 1 shows our present comparative

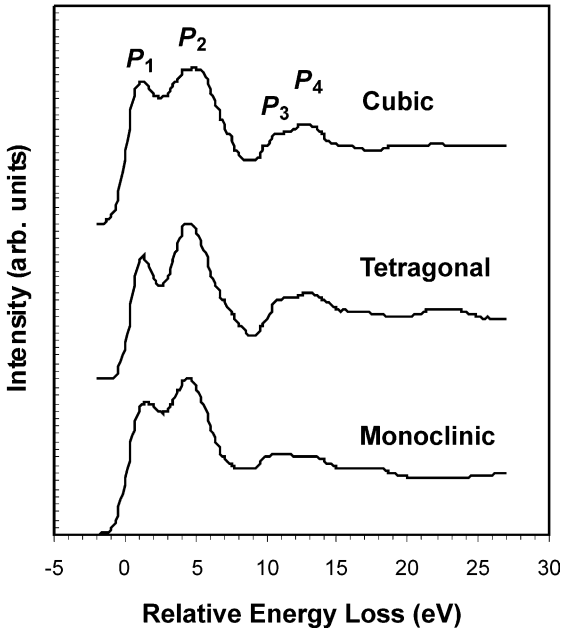

Fig. 1. Comparison of experimental energy-loss near edge structure at the oxygen K-edge for the standard *c*-, *t*- and *m*-ZrO_2 powders. The edges have been aligned by setting the first maximum in the differentiated spectra to 0 eV.

Table 1
Experimental peak energies (eV) from the oxygen K-edge spectra of the standard ZrO_2 powders[a]

Peak	Cubic	Tetragonal	Monoclinic
P_1	1.1	1.0	1.4
P_2	4.7	4.2	4.4
P_3	11.0	11.0	10.5
P_4	12.5	12.7	12.8
ΔE	3.6	3.2	3.0
FWHM	7.6	6.5	7.0

[a] ΔE corresponds to the separation of P_1 and P_2 and the FWHM corresponds to the full width half maximum of the intensity band $P_1 + P_2$ (experimental error ± 0.1 eV).

results of the oxygen K-edge spectra obtained from the standard cubic, tetragonal and monoclinic zirconia powders. The peak energies for the three phases are shown in Table 1. The separation of peaks P_1 and P_2, ΔE, and the shape of the post-edge structure (10–25 eV above the edge onset) were found to be characteristic of each phase. Additionally, if one considers peaks P_1 and P_2 as a single band of intensity, a measurement of the full width at the half maximum (FWHM) of this intensity band provides an even more precise means of distinguishing between different phases in good agreement with the earlier results of McComb.[6]

Examination of a polished and thermally etched sintered compact in the scanning electron microscope (JEOL 6400) revealed a bimodal microstructure shown in Fig. 2, consisting of large grains approximately $\geqslant 1$ μm in size within a finer matrix having an average grain size of 0.3 μm. Such a microstructure can arise as a consequence of variations in Y_2O_3 distribution within the starting powder which does not homogenise during sintering, or as a result of sintering in the tetragonal plus cubic phase fields. In both cases, this results in a predominantly t-ZrO_2 matrix with a small fraction of c-ZrO_2 generally present as the larger grains.[3,9]

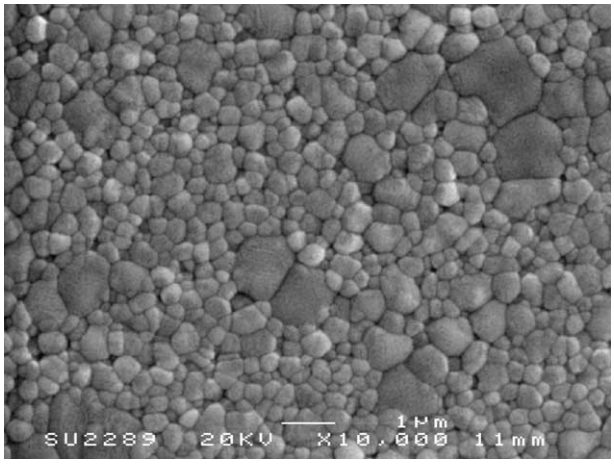

Fig. 2. SEM micrograph revealing the bimodal grain structure within the 3Y-TZP derived from the Tioxide YZ5N co-milled powder.

A typical region of the specimen consisting of predominantly smaller t-ZrO_2 is shown in Fig. 3(a) and a large grain, believed to be c-ZrO_2, is shown in Fig. 3(c) with the corresponding SAED patterns given in Fig. 3(b) and (c) respectively. The tetragonal distortion from the cubic *fluorite* structure is relatively small ($c/a \approx 1.016$) and hence it is often problematic to distinguish between the tetragonal and cubic phases using conventional electron diffraction in the TEM. Tilting of specific grains to a number of different zones was used to confirm the assignment of the grains selected for further investigation.

Fig. 4(a) and (b) show the yttrium and zirconium $L_{2,3}$ edges obtained from the large grain "Y" and small grain "X" shown in Fig. 3(a) and (d) respectively. Quantification gave Y/Zr atomic ratios of 0.16 ± 0.025 and 0.045 ± 0.007 for the large grain and small grain respectively. The increase in the relative Y/Zr ratio exhibited by the spectrum shown in Fig. 4(a) supports the proposition that the larger grains are c-ZrO_2. The corresponding oxygen K-edge spectra are given in Fig. 5(a) and (b). The peak positions, the shape of the high energy ELNES some 10–20 eV above the edge onset and the values of the FWHM ($P_1 + P_2$) of 7.5 eV and 6.4 eV for the large and small grains respectively, clearly differentiates the c-ZrO_2 and t-ZrO_2 phases respectively (see Table 1), consistent with the work of McComb.[6]

For high purity Y–ZrO_2, it has been shown that the separation of P_1 and P_2 (ΔE) is directly related to the metal fraction of yttrium present.[14] Interestingly, examination of the ELNES of the oxygen K-edge sampled from different positions within a single grain or from different grains of similar size revealed slight variations in the separation of peaks P_1 and P_2, (ΔE) between 3.0 and 3.3 eV. This too is likely to be a consequence of local differences in the stabiliser concentration and is consistent with the results of corresponding EDX microanalysis which showed variations in the Y/Zr atomic ratio between 0.06 and 0.13 for adjacent grains of a similar size, an inherent property of TZP ceramics prepared from the mixed oxide route.[15] Moreover, some small grains (<0.5 μm in size) exhibited O K-edge ELNES (and corresponding Y/Zr ratios) characteristic of the c-ZrO_2 phase illustrating the need for caution when interpreting the structure based on morphology alone.

TEM analysis also revealed that occasionally grains close to the edge of the hole in the ion beam thinned specimen displayed a twinned m-ZrO_2 structure such as that illustrated in Fig. 6. From the twin morphology,[1] and since they were only found at the specimen edge, these grains were believed to be originally t-ZrO_2, with transformation to m-ZrO_2 induced during specimen preparation. An oxygen K-edge spectrum from such a grain is shown in Fig. 5(c). Examination of the ELNES within Fig. 5(c) shows a separation of peaks P_1 and P_2,

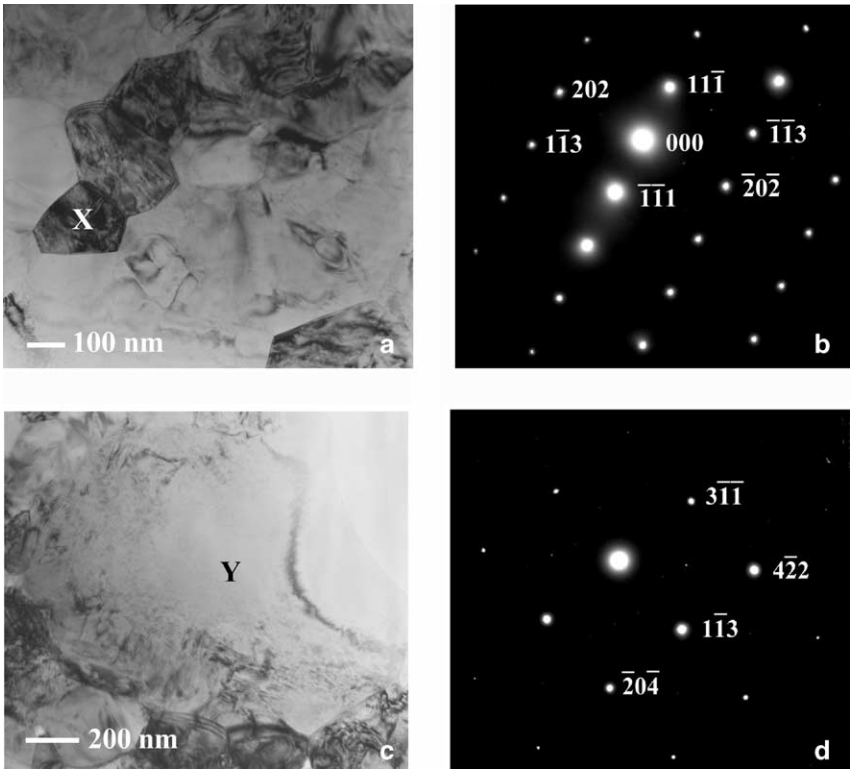

Fig. 3. (a) Bright-field TEM image of a cluster of small grains (b) corresponding SAED pattern from the grain "X" tilted to a t-ZrO_2 [$\bar{1}$, 2, 1] zone (c) typical large grain "Y" with a corresponding SAED pattern shown in (d) indexed to a to a c-ZrO_2 [2, $\bar{5}$, 1] zone.

ΔE, of 3.1 eV. The distinction between the t-ZrO_2 and m-ZrO_2 based on the separation of peaks P_1 and P_2 was not as obvious as that observed for the standard powders. This is not surprising given that the m-ZrO_2 powders used contained no Y^{3+}, while the grain in Fig. 6 clearly did. However, the shape of the post-edge structure in Fig. 5c (particularly the reduction in the peak intensity 20–25 eV above the edge onset) clearly exhibits the distinctive characteristics expected from the monoclinic phase. Moreover, the FWHM of 7.1 eV is consistent with m-ZrO_2. The Y/Zr atomic ratio, calculated from the corresponding Y and Zr $L_{2,3}$-edges gave a value of 0.031 ± 0.01. This corresponds to an Y_2O_3 concentration of $\sim$1.6 mol% which is unlikely to be sufficient to stabilize t-ZrO_2 in an unconstrained grain.[16]

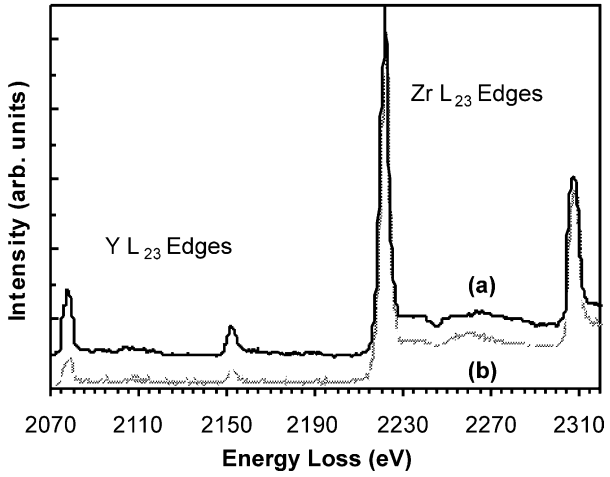

Fig. 4. Yttrium and zirconium $L_{2,3}$ edges from a typical (a) large grain "Y", and (b) small grain "X" (spectra normalised to the Zr L_3 edge, and y axis off-set for clarity).

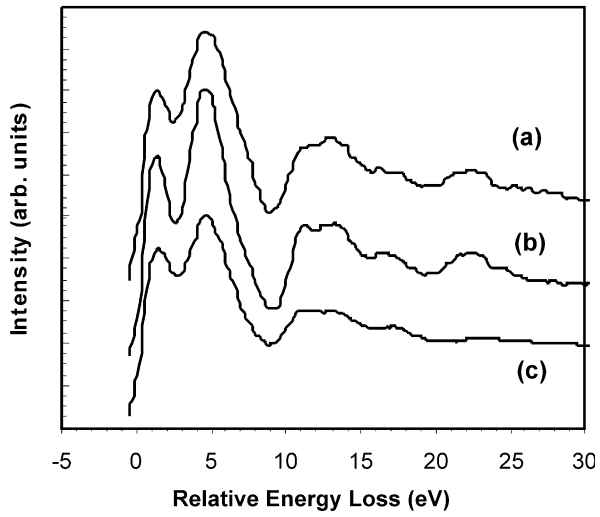

Fig. 5. The corresponding oxygen K-edge spectra for the (a) large grain, and (b) small grain shown in Fig. 3(d) and (a) respectively and (c) transformed grain shown in Fig. 6 (edges have been aligned at the first maximum in the differentiated spectra and vertically offset for clarity).

Hence, the evidence provided by EELS and the ELNES is consistent with the observation that this grain transformed from t-ZrO_2 to m-ZrO_2, most likely as a consequence of damage induced during TEM specimen preparation, while surrounding grains, that were richer in Y^{3+}, were unaffected.

3.2. Comparison of grain boundaries to near grain boundary regions

Many commercial yttria-stabilised zirconia ceramics are known to contain significant quantities of other additions present, either as processing impurities or added intentionally for example: to improve the densification during sintering (e.g. Al_2O_3, SiO_2), or to increase the t-$ZrO_2 \rightarrow m$-ZrO_2 transformation temperature (e.g. HfO_2). It is generally recognised that many of these dopants, including the Y^{3+} stabiliser itself, undergo significant segregation to the free surface and grain boundary regions under certain conditions.[17–20] To further examine this phenomenon with our current material, extensive spatially resolved EELS and EDX nano-probe (1 nm) analysis was performed on numerous grain boundaries and their corresponding near grain-boundary (NGB) grain-interiors (5–10 nm from the boundary interface). Boundaries were aligned approximately edge-on to the electron beam and were chosen from regions of the specimen containing predominantly smaller grains. Results from boundaries adjacent to likely cubic grains, i.e. grain interiors which exhibited a Y/Zr atomic ratio higher than 0.11 and showing a corresponding ELNES at the oxygen K-edge indicative of the cubic phase, were ignored.

The Y/Zr atomic ratios obtained from typical NGB grain interiors ranged from 0.045 to 0.10 ± 0.01. However, the grain boundaries exhibited enhanced Y^{3+} concentrations with Y/Zr atomic ratios up to 0.19 ± 0.04, the full data set being presented elsewhere.[9] Another interesting difference between grain boundary and NGB was between the Al^{3+} levels. No Al^{3+} could be detected in the NGB, however, corresponding grain boundary interfaces were found to contain significant quantities of Al^{3+} (between 0.6 and 1.4 at.% in a 1 nm probe). The full details of this are reported elsewhere.[9]

Fig. 7 shows an oxygen K-edge spectrum taken from a NGB grain interior and an adjacent grain boundary. The main features in the near-edge fine structure are almost identical in both spectra suggesting that oxygen atoms at the boundary are in a similar environment to the oxygen atoms within the bulk grains. This strongly suggests that both the grain boundary and the near-grain interiors investigated possessed a tetragonal-ZrO_2 symmetry. This is, of course, consistent with the absence of any phase boundary in the grain boundary region. Nevertheless, this result is quite surprising since the concentration of Y^{3+} within the boundary region was often equivalent or greater than that found within the large cubic grains observed within the bulk of the material.

The ELNES at the oxygen K-edge, obtained from several data sets, gave a mean peak separation between P_1 and P_2, ΔE, of 3.1 ± 0.1 eV and a FWHM of $P_1 + P_2$ of 6.8 ± 0.2 eV for the NGB. The corresponding values for the grain boundary regions gave a peak separation, ΔE of 3.1 ± 0.1 eV and a FWHM of $P_1 + P_2$ of 7.0 ± 0.3 eV. While there was little variation in the peak separation, ΔE, between the NGB and grain boundary region a slight increase in the value of the FWHM of $P_1 + P_2$ for both the NGB and grain boundary region, relative to the bulk grain was observed. The cause of this broadening in the intensity band $P_1 + P_2$ is not entirely clear but was particularly distinct for boundaries containing relatively higher Al^{3+} concentrations. Vlachos et al.[14] show the value of the separation of P_1 and P_2,

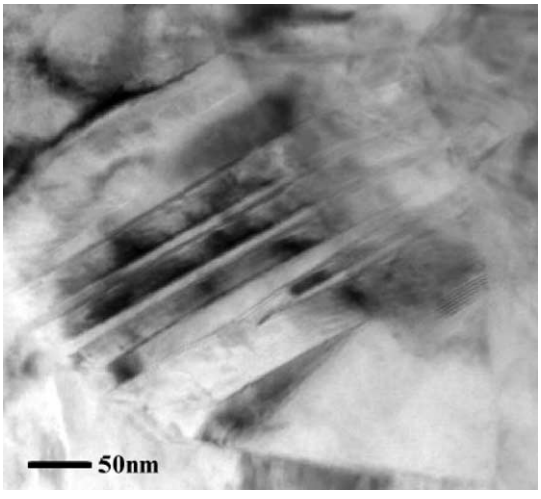

Fig. 6. (a) Bright-field TEM image showing the martensitic twins within a transformed grain.

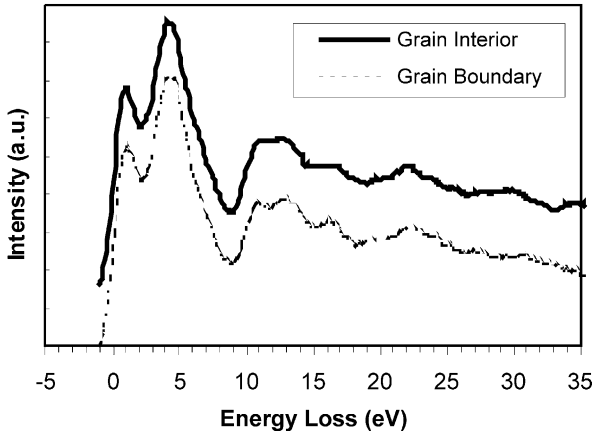

Fig. 7. ELNES at the oxygen K-edge from a near boundary grain-interior (solid line) and corresponding grain boundary (dashed line) (spectra have been aligned at the first maximum in the differential spectra and vertically offset for clarity).

ΔE, in ELNES and parallel X-ray absorption near edge structure (XANES) studies, is related approximately linearly to the Y concentration. The peak separation measured in the current work is slightly smaller than that obtained by Vlachos et al. However, Vlachos et al. examined thermodynamically stable powders while the current work was for metastable t-ZrO_2. The current results are therefore not considered to be totally inconsistent with those of Vlachos et al.

There have been a number of observations[18,19,21–24] of Y^{3+} segregation to grain boundaries in both t-ZrO_2 and c-ZrO_2, where no change in grain boundary structure was observed. However, examination of the local bonding configuration via ELNES studies has been generally limited to specific c-ZrO_2: c-ZrO_2 grain boundaries. For example, Dickey et al.[19] reported an increase in the Y^{3+} concentration at a $\Sigma 5$ grain boundary within a specially prepared cubic YSZ bicrystal ($\sim$10 mol% Y_2O_3). Although in their work the Y/Zr atomic ratio was significantly higher at the grain boundary (0.291 ± 0.002) with respect to the bulk grain (0.161 ± 0.002), no difference was observed in the ELNES at the oxygen K-edge. Thus, while this latter study concentrated on an ideal single boundary within the cubic system their work does suggest that certain c-ZrO_2: c-ZrO_2 grain boundaries can also accommodate a higher stabiliser content without appearing to change the local oxygen atomic environment as reflected in the ELNES at the oxygen K-edge.

The segregation of Y^{3+} and Al^{3+} to the grain boundary region will modify the space charge layer. The precise structure of the space charge region is not known with certainty because of the need to probe atomic positions, bond lengths, vacancy distributions and consequently lattice strain energy on the nm scale. Rough estimates of the width of the space charge layer can be made from impedance measurements.[25,26] For a similar TZP to the one examined here,[27] a value of $\sim$4 nm is estimated, but of course, the grain boundary layer itself is only a single atom layer. While models have been proposed (e.g. see ref 28), experimental verification has not, as yet, been provided. In any event, the spatial resolution of our current EELS measurements is of the order of the space charge layer size, and it is therefore probable that recorded energy-loss spectra represent an average of the oxygen atomic environments within the grain boundary region. For a nominal 1 nm electron probe we estimate that, very approximately, only 25–50% of the oxygen species within the sample volume are located at the grain boundary (for a 2 nm probe this drops to 13–25%). Therefore, the absence of any major changes between the bulk and grain boundary oxygen K-edge ELNES may simply indicate that the spatial resolution was insufficient to detect any localised differences in the oxygen environment within the space-charge layer and boundary interface or, that the net effect of the various space-charge components is below the energy resolution of the current EEL spectrometer. The prospects of future studies using aberration corrected sub-Angstrom STEM probes (e.g. UK SuperSTEM facility at Daresbury Laboratories) may resolve this matter. However, the present results certainly show that the relationship between the cation dopant concentration and ELNES at the oxygen K-edge for grain boundary regions behaves differently to that of the bulk grain interiors. Therefore, there is a clear need to measure and theoretically model these boundaries in more detail. Such modelling should take into account the changes in localised oxygen coordination, the presence of segregated cations ions and the location of oxygen vacancies, if a complete understanding of the grain boundary structures in 3Y-TZPs and resulting oxygen K-edge ELNES is to be achieved.

4. Conclusions

In this brief report we have confirmed the use of EELS and ELNES as a powerful tool for the determination of the structural morphology of bulk grains within 3Y-TZPs. Analysis of the positions and FWHM of peaks P_1 and P_2, and the shape of the post edge fine structure clearly facilitates a rapid means of differentiation between the cubic, tetragonal and monoclinic phases. Significant co-segregation of Y^{3+} and Al^{3+} has been observed at the grain boundary interface for the co-milled 3Y-TZP containing 0.15 wt.% Al_2O_3 additions. Examination of the ELNES at the oxygen K-edge for typical t-ZrO_2: t-ZrO_2 grain boundaries suggest that, irrespective of strong cation co-segregation, the oxygen coordination at the boundary interface is, on average, similar to that of the bulk tetragonal grains for the volume sampled by the electron beam.

Acknowledgements

The authors gratefully acknowledge support for this research from the Engineering and Physical Sciences Research Council (EPSRC Grants GR/M50089, GR/M50096 and GR/M50089/01), Tioxide Specialities and Dynamic Ceramic Ltd.

References

1. Lee, W. E. and Rainforth, W. M., *Ceramic Microstructures*. Chapman and Hall, 1994.
2. Green, D. J., Hannink, R. H. J. and Swain, M. V., *Transformation Toughening of Ceramics*. CRC Press, 1989.
3. Singh, R., Gill, C., Lawson, S. and Dransfield, G. P., Sintering, microstructure and mechanical properties of commercial Y-TZP's. *J. Mat. Sci.*, 1996, **31**, 6055–6062.

4. Srinivasan, R., Deangelis, R. J., Ice, G. and Davis, B. H., Identification of tetragonal and cubic structures of zirconia using synchrotron X-radiation source. *J. Mater. Res.*, 1991, **6**, 1287.
5. Selulic, A., Furick, K., Tonejc, A., Tonejc, A. M. and Stubicar, M., Determination of the monoclinic, tetragonal and cubic phases in mechanically alloyed ZrO_2–Y_2O_3 and ZrO_2–CoO powder mixtures by Raman spectroscopy. *J. Mat. Sci. Lets.*, 1997, **16**, 260–262.
6. McComb, D. W., Bonding and electronic structure in zirconia pseudopolymorphs investigated by electron energy-loss spectroscopy. *Phys. Rev. B*, 1996, **54**, 7094–7102.
7. Stemmer, S., Vleugels, J. and Van-Der Biest, O. J., Grain boundary segregation in high-purity yttria-stabilized tetragonal zirconia polycrystals (Y-TZP). *Eur. Ceram. Soc.*, 1998, **18**, 1565–1570.
8. Yuan, J., Hirayama, T., Ikuhara, Y. and Sahuma, T., Electron energy loss spectroscopy study of cerium stabilised zirconia: an application of valence determination in rare earth systems. *Micron*, 1999, **30**, 141–145.
9. Ross, I. M., Rainforth, W. M., McComb, D. W., Scott, A. J. and Brydson, R., The role of trace additions of alumina to yttria–tetragonal zirconia polycrystals (Y-TZP). *Scripta Mater.*, 2001, **45**, 653–660.
10. Appel, C. C., Botton, G. A., Horsewell, A. and Stobbs, W. M., Chemical and structural changes in manganese-doped yttria stabilized zirconia studied by electron energy-loss spectroscopy combined with electron diffraction. *J. Am. Ceram. Soc.*, 1999, **82**, 429–435.
11. Brydson, R., Probing the local structure and bonding at interfaces and defects using EELS in the TEM. *J. Micros.*, 1995, **180**, 238–249.
12. Ostanin, S., Craven, A. J., McComb, D. W., Vlachos, D., Alavi, A., Finnis, M. W. and Paxton, A. T., Effect of relaxation on the oxygen K-edge electron energy loss near-edge structure in yttria-stabilized zirconia. *Phys. Rev. B*, 2000, **62**, 14728–14733.
13. Egerton, R. F., *Electron Energy Loss Spectroscopy in the Electron Microscope*. Plenum, New York, 1996.
14. Vlachos, D., Craven, A. J. and McComb, D. W., The influence of dopant concentration on the oxygen K-edge ELNES and XANES in yttria-stabilized zirconia. *J. Phys.: Condens. Matter.*, 2000, **13**, 10799–10809.
15. Burke, D., *Low Temperature Degradation of Yttria Stabilised Tetragonal Zirconia Polycrystals (TZP's)*, PhD Thesis, University of Sheffield, 1998.
16. Miller, R., Smialek, A. and Garlick, R. G., In *Advances in Ceramics, Volume 3, Science and Technology of Zirconia*, ed. A. H. Heuer and L. W. Hobb. American Ceramic Society, OH, 1981.
17. Ross, I. M., Rainforth, W. M., McComb, D. W., Scott, A. J. and Brydson, R., Grain boundary segregation in Al_2O_3 doped 3Y-TZP ceramics. *Inst. Phys. Conf. Ser.*, 2001, **168**, 299–302.
18. Hwang, S. L. and Chen, I. W., Grain size control of tetragonal zirconia polycrystals using the space charge concept. *J. Am. Ceram. Soc.*, 1990, **73**, 3269–3277.
19. Dickey, E. C., Fan, X. and Pennycook, S. J., Structure and chemistry of yttria-stabilized cubic-zirconia symmetric tilt grain boundaries. *J. Am. Ceram. Soc.*, 2001, **84**, 1361–1368.
20. Shibata, N., Oba, F., Yamamoto, T., Ikuhara, Y. and Sakuma, T., Atomic structure and solute segregation of a $\Sigma = 3$, [110]/{111} grain boundary in an yttria-stabilised cubic zirconia bicrystal. *Phil. Mag. Lett.*, 2002, **82**, 393–400.
21. Winnubst, A. J. A., Kroot, P. J. M. and Burggraaf, A. J., AES/STEM grain boundary analysis of stabilised zirconia ceramics. *J. Phys. Chem. Solids*, 1983, **44**, 955–960.
22. Theunissen, G. S. A. M., Winnubst, A. J. A. and Burggraaf, A. J., Surface and grain boundary analysis of doped zirconia ceramics studied by AES and XPS. *J. Mater. Sci.*, 1992, **27**, 5057–5066.
23. Nieh, T. G. and Wadsworth, J., Superplastic behaviour of a fine-grained yttria-stabilized, tetragonal zirconia polycrystal (Y-TZP). *Acta Metall. Mater.*, 1990, **38**, 1121–1133.
24. Ikuhara, Y., Thavorniti, P. and Sakuma, T., Solute segregation at grain boundaries in superplastic SiO_2-doped TZP. *Acta Mater.*, 1997, **45**, 5275–5284.
25. Guo, X., Solute segregation at the space-charge layers of stabilised zirconia: an opportunity for ameliorating conductivity. *J. Eur. Ceram. Soc.*, 1996, **16**, 575–578.
26. Guo, X., Size dependent grain-boundary conductivity in doped zirconia. *Comp. Mater. Sci.*, 2001, **20**, 168–176.
27. Rodriquez-Pulido, A., Abraham, E., Ross, I. M. and Rainforth, W. M., The effect of small alumina additions to Y-TZPs. *J. Mater. Sci.* (Submitted for publication).
28. Yan, M. F., Cannon, R. M. and Bowen, H. K., Space-charge, elastic field, and dipole contributions to equilibrium solute segregation at interfaces. *J. Appl. Phys.*, 1983, **54**, 764–778.